Towards a simple representation of chalk hydrology in land surface modelling

Mostaquimur Rahman[1], Rafael Rosolem[1,2]

[1]Department of Civil Engineering, University of Bristol, Bristol, UK

[2]Cabot Institute, University of Bristol, Bristol, UK

Abstract

Modelling and monitoring of hydrological processes in the unsaturated zone of chalk, a porous medium with fractures, is important to optimize water resources assessment and management practices in the United Kingdom (UK). However, incorporating the processes governing water movement through chalk unsaturated zone in a numerical model is complicated mainly due to the fractured nature of chalk that creates high-velocity preferential flow paths in the subsurface. In general, flow through chalk unsaturated zone is simulated using dual-porosity concept, which often involves calibration of relatively large number of model parameters, potentially undermining applications to large regions. In this study, a simplified parameterization, namely the Bulk Conductivity (BC) model is proposed for simulating hydrology in chalk unsaturated zone. This new parameterization introduces only two additional parameters (namely the macroporosity factor and the soil wetness threshold parameter for fracture flow activation) and uses the saturated hydraulic conductivity from chalk matrix. The BC model is implemented in the Joint UK Land Environment Simulator (JULES) and applied to a study area encompassing the Kennet catchment in the Southern UK. This parameterization is further calibrated at a point-scale using soil moisture profile observations. The performance of calibrated BC model in JULES is assessed and compared against the performance of both the default JULES parameterization and the uncalibrated version of BC model implemented in JULES. Finally, the model performance at the

catchment-scale is evaluated against independent data sets (e.g., runoff and latent heat flux). The results demonstrate that the inclusion of the BC model in JULES improves simulated land surface mass and energy fluxes over the chalk-dominated Kennet catchment. Therefore, the simple approach described in this study may be used to incorporate the flow processes through chalk unsaturated zone in large-scale land surface modelling applications.

Keywords: Chalk hydrology, macroporosity, land surface model, bulk conductivity model.

1. Introduction

Chalk can be described as a fine-grained porous medium traversed by fractures [*Price et al.*, 1993]. Previous studies showed that the unsaturated zone of the chalk aquifers plays an important role on groundwater recharge in the UK [e.g., *Lee et al.*, 2006; *Ireson et al.*, 2009]. Therefore, both monitoring [e.g., *Bloomfield*, 1997; *Ireson et al.*, 2006] and modelling [e.g., *Bakopoulou*, 2015; *Brouyère*, 2006; *Ireson and Butler*, 2011, 2013; *Sorensen et al.*, 2014] strategies have been adapted previously to understand the governing hydrological processes in the chalk unsaturated zone.

In chalk, the matrix provides porosity and storage capacity, while the fractures greatly enhance permeability [*Van den Daele et al.*, 2007]. Water movement through chalk matrix is slow due to its relatively high porosity (0.3-0.4) and low permeability (10^{-9}-10^{-8} ms^{-1}). A fractured chalk system, in contrast, conducts water at a considerably higher velocity because of relatively high permeability (10^{-5}-10^{-3} ms^{-1}) and low porosity (of the order 10^{-4}) of fractures [*Price et al.*, 1993].

Simulating water flow through the matrix-fracture system of chalk has been the subject of research for some time. Both conceptual [e.g., *Price et al.*, 2000; *Haria et al.*, 2003] and physics-based [e.g., *Mathias et al.*, 2006; *Ireson et al.*, 2009] models have been proposed previously to describe water flow through chalk unsaturated zone. The physics-based models mentioned above were developed based on dual-continua approach and required relatively

large numbers of parameters (i.e., on the order of 20-30 parameters) that were calibrated via inverse modelling using observed soil moisture and matric potential data [e.g., *Ireson et al.*, 2009; *Mathias et al.*, 2006].

In recent years, representation of chalk has gained attention in land surface modelling. For example, *Gascoin et al.* [2009] applied the Catchment Land Surface Model (CLSM) over the Somme River basin in northern France. A linear reservoir was included in the TOPMODEL based runoff formulation of CLSM to account for the contribution of chalk aquifers to river discharge. *Le Vine et al.* [2016] applied the Joint UK Land Environment Simulator (JULES [*Best et al.*, 2011]) over the Kennet catchment in southern England to evaluate the hydrological limitations of land surface models. In that study, two intersecting Brooks and Corey curves were proposed, which allowed a dual curve soil moisture retention representation for the two distinct flow domains of chalk (i.e., matrix and fracture) in the model. Considering this dual Brooks and Corey curve, a three-dimensional groundwater flow model (ZOOMQ3D [*Jackson and Spink*, 2004]) was coupled to JULES to demonstrate the strong influence of representing chalk hydrology and groundwater dynamics on simulated soil moisture and runoff.

The above mentioned studies illustrate the importance of representing chalk in land surface modelling. However, including chalk hydrology in large-scale land surface modelling using the contemporary dual-porosity concept can be complicated due to large number of additional parameters. In this context, we propose a new parameterization, namely the Bulk Conductivity (BC) model as a first step towards a simple chalk representation suitable for land surface modelling. In order to test the proposed parameterization, the BC model is included in JULES (version 4.2), which, by default (i.e., uniform soil column representation using general soil database as typically applied in land surface models), does not represent any chalk feature. In this study, the BC model (included in JULES) is applied at two distinct

spatial scales (i.e., point and catchment). At the point-scale, the proposed parameterization is calibrated using observed soil moisture profile data. This is achieved by randomly sampling the parameter space and extensively running the model in order to minimize the differences between observed and simulated soil moisture variability at different depths. Finally, the proposed model is applied to the Kennet catchment in the Southern England and the fluxes and states of the hydrological cycle are simulated for multiple years. The simulation results are evaluated using observed latent heat flux (LE) and runoff data to assess the performance of the BC model in simulating land surface processes at the catchment scale.

2. A model of flow through chalk unsaturated zone

In this study, the *Bulk Conductivity* (BC) model based on the work by *Zehe et al.* [2001] is incorporated in JULES to represent the flow of water through the fractured chalk unsaturated zone. According to this approach, if the relative saturation (S) exceeds a certain threshold (S_0) at a soil grid, the saturated hydraulic conductivity of chalk matrix (K_s) is increased to a bulk saturated hydraulic conductivity (K_{sb}) as follows

$$K_{sb} = K_s + K_s f_m \frac{S - S_0}{1 - S_0} \qquad \text{if } S > S_0 \tag{1}$$

$$K_{sb} = K_s \qquad \text{if } S <= S_0 \tag{2}$$

with $S = \frac{\theta - \theta_r}{\theta_s - \theta_r}$

where f_m is a macroporosity factor (-), θ is soil moisture (m^3m^{-3}), θ_s is soil moisture at saturation (m^3m^{-3}) and θ_r is the residual soil moisture (m^3m^{-3}). Note that S ranges from zero in case of completely dry soils to one for fully wet soils.

At the first step of evaluation, the K_s, S_0 and f_m parameters are estimated based on existing literature to assess the performance of the uncalibrated BC model. For the matrix saturated hydraulic conductivity (K_s), we use K_s = 1.0 mmd^{-1} following *Mathias et al.* [2006]. In

addition, Equation 1 indicates that the onset of water flow through the fracture system of chalk is controlled by the threshold S_0. According to *Wellings and Bell* [1980], water flow through fractures dominates over matrix flow in chalk when the pressure head in soil becomes higher than -0.50 mH_2O. We consider a value of $S_0 = 0.80$ for the uncalibrated BC model, which is based on observed soil moisture-matric potential relationship in the study area.

Finally, In *Zehe et al.* [2001], f_m was defined as the ratio of the saturated water flow rate in all macropores in a model element to the corresponding value in soil matrix, which can be determined based on the density and length of fractures at small scales. In addition, f_m has also been considered as a calibration parameter previously [e.g., *Blume*, 2008; *Zehe et al.*, 2013]. In this study, we define f_m as a characteristic soil property reflecting the influence of fractures on soil water movement [*Zehe and Blöschl*, 2004] and estimate it from the relative difference of permeability between chalk matrix and fractured chalk system that can be of the order 10^4-10^6 according to *Price et al.* [1993]. Consequently, we consider a macroporosity factor of $f_m = 10^5$ for the uncalibrated BC model. In the following step, the BC model is calibrated to minimize the differences between the variability of observed and simulated soil moisture at individual depths. The calibration strategy will be discussed elaborately in section 3.5.

3. Methods

3.1. Study area

The study area encompasses the Kennet catchment located in the Southern England with an area of about 1033 km^2 (Figure 1a). Generally, Kennet is rural in nature with scattered settlements and has a maximum altitude of approximately 297 m (Above Ordnance Level). The River Kennet discharges into the North Sea through London. The major tributaries of

this river are Lambourn, Dun, Enborne, and Foudry Brook. An average annual rainfall of approximately 760 mm was recorded in the catchment over a 40 year period from 1961-1990.

Solid geology of the Kennet catchment is dominated by chalk, which is overlain by thin soil layer. While lower chalk outcrops along the northern catchment boundary, progressively younger rocks are found in the southern part. In general, surface runoff production is very limited over the regions of the catchment where chalk outcrops. The flow regime shows a distinct characteristics of slow response to groundwater held within the chalk aquifer [*Le Vine et al.*, 2016]. According to *Ireson and Butler* [2013], the unsaturated zone of chalk shows slow drainage over summer and bypass flow during wet periods in this catchment.

3.2. Field measurements and remotely sensed data

Table 1 summarizes the field measurements and remote sensing data used in this study. We use *in-situ* soil moisture and runoff measurements along with remotely sensed LE data to assess model performance in simulating the mass and energy balance components of the hydrological cycle. Point scale soil moisture measurements at two adjacent sites (~20 m apart) at the Warren Farm (Figure 1) were provided by Centre for Ecology and Hydrology (CEH). A Didcot neutron probe was used at these locations to measure fortnightly soil moisture at different depths below land surface (10 cm apart down to 0.8 m, 20 cm apart between 0.8-2.2 m, and 30 cm apart between 2.2-4.0 m) [*Hewitt et al.*, 2010].

The National River Flow Archive (NRFA) coordinates discharge measurements from the gauging station networks across UK. These networks are operated by the Environmental Agency (England), Natural Resources Wales, Scottish Environment Protection Agency, and Rivers Agency (Northern Ireland). We use discharge measurements provided by NRFA to assess model performance in simulating runoff over the Kennet catchment in this study.

The MOD16 product of the Moderate Resolution Imaging Spectroradiometer (MODIS) is a part of NASA/EOS project that provides estimation of global terrestrial LE. The LE estimation from MOD16 is based on remotely sensed land surface data [e.g., *Mu et al.*, 2007]. In this study, the 8-day and monthly LE data products from MODIS is used to evaluate the model performance in simulating land surface energy fluxes.

3.3. Land surface model

In this study, we use the Joint UK Land Environment Simulator (JULES [e.g., *Best et al.*, 2011; *Clark et al.*, 2011]) version 4.2. JULES is a flexible modelling platform with a modular structure aligned to various physical processes developed based on the Met Office Surface Exchange Scheme (MOSES [e.g., *Cox et al.*, 1999; *Essery et al.*, 2003]). Meteorological data including precipitation, incoming short- and longwave radiation, temperature, specific humidity, surface pressure, and wind speed are required to drive JULES. Each grid box in JULES can comprise nine surface types (broadleaf trees, needle leaf trees, C3 grass, C4 grass, shrubs, inland water, bare soil, and ice) represented by respective fractional coverage. Each surface type is represented by a tile and a separate energy balance is calculated for each tile.

Subsurface heat and water transport equations are solved based on finite difference approximation in JULES as described in *Cox et al.* [1999]. Moisture transport in the subsurface is described by the finite difference form of Richards' equation. The vertical soil moisture flux is calculated using the Darcy's law. While the top boundary condition to solve the Richards' equation is infiltration at soil surface, the bottom boundary condition in JULES is free drainage that contributes to subsurface runoff.

Surface runoff is calculated by combining the equations of throughfall and grid box average infiltration in JULES. In order to direct the generated runoff to a channel network, river routing is implemented based on the discrete approximation of one-dimensional kinematic

wave equation [e.g., *Bell et al.*, 2007]. In this approach, river network is derived from the digital elevation model (DEM) of the study area and different wave speeds are applied to surface and subsurface runoff components and channel flows [e.g., *Bell and Moore*, 1998]. A return flow term accounts for the transfer of water between subsurface and land surface [e.g., *Dadson et al.*, 2010, 2011].

3.4. Model configurations and input data

In this study, simulations are performed at two distinct spatial scales, namely point and catchment. At the point scale, JULES is configured to simulate the mass and energy fluxes at the Warren Farm site (Figure 1a). A total subsurface depth of 5 m is considered in the model with a vertical discretization ranging from 10 cm at the land surface to 50 cm at the bottom of the model domain. Note that this discretization is consistent with the soil moisture measurement depths mentioned in section 3.2. The vegetation type is implemented as C3 grass using the default parameters in JULES. Point scale simulations were performed over 2 consecutive years from 2003-2005 at an hourly time step. Except for precipitation, hourly atmospheric forcing data to drive JULES was obtained from an automatic weather station operated by the CEH at Warren Farm. In order to estimate hourly precipitation data to run JULES, rain gauge measurements from the Met Office [*Met Office*, 2006] were used. Inverse distance interpolation technique [e.g. *Garcia et al.*, 2008; *Ly et al.*, 2013] was applied on rainfall measurements from 13 gauges closest to Warren Farm (distance varies from 25-60 km) to obtain hourly precipitation for the point scale simulations.

At the catchment scale, JULES is configured over a study area encompassing the Kennet catchment (Figure 1a) considering a uniform lateral grid resolution of 1 km with 70 x 40 cells in x and y dimensions, respectively. The total subsurface depth and vertical discretization are identical to those of the point scale simulations. Spatially distributed vegetation type

193 information for the study area (Figure 1b) is obtained from the Land Cover Map 2007
194 (LCM2007) dataset [*Morton et al.*, 2011]. Simulations were performed over 5 consecutive
195 years from 2006-2011 at the catchment scale. Note that the simulation periods of catchment
196 and point scale (2003-2005) do not coincide due to the availability of soil moisture
197 measurements described in section 3.2. Spatially distributed meteorological data from the
198 Climate, Hydrology and Ecology research Support System (CHESS) was used to obtain the
199 atmospheric forcing to drive JULES at the catchment scale. The CHESS data includes 1 km
200 resolution gridded daily meteorological variables [*Robinson et al.*, 2015]. This daily data is
201 downscaled using a disaggregation technique described in *Williams and Clark* [2014] to
202 obtain hourly atmospheric forcing. The flow direction required for river routing is extracted
203 from the USGS HydroSHEDS digital elevation data [*Lehner et al.*, 2008].

204 We estimate the soil hydraulic properties based on texture (Table 2). At the point scale, loam
205 soil is dominant at the Warren Farm site. At the catchment scale, the Harmonized World Soil
206 Database (HWSD) from the Food and Agricultural Organization of UNO (FAO) is used to
207 obtain the texture of different soil types over Kennet (Figure 1c). The saturation-pressure
208 head relationship for different soil types is described using the Van Genuchten [*Van*
209 *Genuchten*, 1980] model with parameter values (Table 2) obtained from *Schaap and Leij*
210 [1998].

211 The hydraulic properties for chalk used in this study are summarized in Table 3. These
212 properties are obtained based on existing literature as a first step when evaluating the
213 uncalibrated BC model. The BC model parameters are subsequently calibrated to minimize
214 the differences between observed and simulated $\Delta\theta$ (section 3.5) at various soil depths.

215 In this study, we consider two different model configurations, namely *default* and *macro*
216 (Figure 2). The *default* configuration corresponds to the standard parameterizations of JULES

that does not represent chalk hydrology in the model. In this configuration, each soil column in JULES is considered to be vertically homogeneous with the soil properties defined in Table 2, which is motivated by the Met Office JULES Global Land 4.0 configuration described in *Walters et al.* [2014]. The *macro* configuration, in contrast, explicitly represents chalk by applying the BC model starting at 30 cm below land surface to the bottom of the model domain (i.e. 500 cm). Therefore, the soil column in the *macro* configuration can be divided into topsoil (0-30 cm) and chalk (30-500 cm). The topsoil depth of 30 cm is defined based on several augured soil samples collected during a field campaign at Warren Farm in 2015 (Figure 2). This depth is corroborated by additional information from the British Geological Survey (BGS) operated borehole records (http://www.ukso.org/pmm/soil_depth_samples_points.html), which show that topsoil depths vary from 10-40 cm over the study area. We apply the *macro* configuration assuming a spatially homogeneous topsoil depth of 30 cm for both point and catchment scale simulations. Note that except for this inclusion of chalk, *default* and *macro* configurations are identical in terms of model set up and input data. It should also be emphasized that *default* represents a "naïve" configuration deprived of model calibration. Moreover, this configuration does not represent chalk, which, according to previous studies [e.g., *Le Vine et al.*, 2016], substantially affects the hydrology of the study area considered here.

3.5. Calibration of the BC model

We calibrate the BC model at the point-scale to minimize the differences between observed and simulated soil moisture variability ($\Delta\theta$) at different depths. The Root Mean Squared Error (RMSE) is used as the objective function to optimize the BC model parameters [e.g., *Ireson et al.*, 2009]

$$RMSE = \frac{1}{nd}\sum_{1}^{nd}\sqrt{\left(\frac{1}{nt-1}\sum_{2}^{nt}\left(\Delta\theta_{d,t}^{obs} - \Delta\theta_{d,t}^{sim}\right)^2\right)} \quad (3)$$

where *nd* is the number of soil layers, *nt* is the number of soil moisture observations available for a layer *d*, $\Delta\theta^{obs}$ is the observed variability of soil moisture and $\Delta\theta^{sim}$ is the simulated variability of soil moisture. Note that we consider $\Delta\theta$ for this optimization because of its relevance to the water flux and recharge through chalk unsaturated zone [e.g., *Ireson and Butler*, 2011].

Equation (1) reveals that the calibration of the BC model involves optimizing 3 parameters, namely the saturated hydraulic conductivity of chalk matrix (K_s), saturation threshold (S_0) and macroporosity factor (f_m). *Ireson et al.* [2009] suggested a range of 0.2-2.0 mmd^{-1} for K_s. On the other hand, *Price et al.* [1993] argued that in general, K_s is around 3-5 mmd^{-1} for most chalk soils. Therefore, we consider a range of 0.2-5.0 mmd^{-1} in optimizing K_s. We consider S_0 range 0-1, representing the entire physical domain for soil wetness from fully dry to fully wet, respectively. For f_m, a range of 10^4-10^6 is considered, which, as discussed earlier, is consistent with the relative difference between the permeability of fractured chalk and chalk matrix according to *Price et al* [1993]. Latin hypercube sampling technique [e.g., *McKay et al.*, 2016] is used to generate 2,000 random samples for each BC model parameter within the ranges discussed above. Note that for the K_s parameter, the random sampling was performed from a logarithmic distribution [*Ireson et al.*, 2009]. We perform simulations using these random samples and calculate model performance (Equation 3) to select the optimum parameter values for the BC model for each possible parameter combination as discussed in details in the following section.

4. Results and discussion

4.1. Point scale simulations

At the point scale, the simulation results are evaluated using soil moisture observations at the Warren Farm site. Figure 3a compares observed and simulated soil moisture (θ) from the

default and *macro* configurations at 2 m below land surface. Note that the *macro* configuration uses the chalk hydraulic parameters collected from existing literature (Table 3). This figure shows that the *default* configuration considerably underestimates θ throughout the simulation period, which is improved remarkably in case of *macro*. Figure 3b plots observed and simulated soil moisture variability ($\Delta\theta$) from the *default* and *macro* configurations ($\Delta\theta_{default}$ and $\Delta\theta_{macro}$, respectively) at the Warren Farm site. In general, both configurations show discrepancies with observed $\Delta\theta$ with *macro* showing relatively better model performance.

The results show that despite the *macro* configuration improves simulated θ, it shows considerable discrepancies with observed $\Delta\theta$, which is consistent throughout the whole chalk profile (results from other model layers are not shown). In order to minimize the differences between observed and modelled $\Delta\theta$ from the *macro* configuration, we calibrate the BC model following the methodology described in section 3.5. The optimization results are summarized in Figure 4. Note that for each combination considered in the optimization, 2,000 model runs were performed using randomly sampled parameters as discussed in section 3.5. In addition to the *default* and *macro* cases, the calibrated cases in Figure 4 correspond to the results from the model runs yielding the lowest RMSE for each parameter combination evaluated.

The RMSE between observed and simulated $\Delta\theta$ for the model configurations considered in the optimization is shown in Figure 4a. This figure illustrates that the RMSE of the *default* configuration is larger than that of *macro*, indicating better model performance in reproducing $\Delta\theta$ for the latter (corresponding to a reduction of 15% in RMSE compared to the *default* case). Therefore, the uncalibrated BC model (i.e., *macro* configuration) better reproduces the soil moisture variability compared to *default*. Concerning the calibration of single BC model parameters, Figure 4a shows that S_0 results in a 46% reduction of RMSE

compared to the *macro* configuration. Calibrating K_s or f_m individually yields only about 25% reduction of RMSE compared to *macro*.

Optimizing both K_s and S_0 simultaneously shows the largest reduction (50%) of RMSE compared to *macro* which coincides with the total RMSE reduction found when all parameters are calibrated. Arguably, the BC model can be implemented in other chalk regions by constraining only S_0 parameter. Such result could potentially be advantageous for transferability to other regions in the UK in order to assess chalk hydrology at large-scale. However since this is the first time the BC model is introduced, we decide to take a conservative approach and select the *macro* configuration with optimized K_s and S_0 ($macro_{opt}$ hereafter) to simulate chalk hydrology over the study area that ensures best overall model performance.

The lower three panels in Figure 4 presents the BC model parameter values for the *default* and uncalibrated *macro* cases as well as for different combinations of parameters calibrated. The red bars in Figure 4a, b and c highlight the cases in which a given parameter is constrained by optimization. In those cases, the calibrated parameter values are obtained from model runs producing the lowest RMSE. An interesting feature in Figure 4b (calibrating K_s individually) is that the optimization suggests a compensation mechanism in which K_s is increased remarkably in order to physically represent the "effective" flow through the chalk fractures in the BC model. This is not surprising and arguably the simplest way to attempt to improve model performance. For $macro_{opt}$, the values used for K_s is relatively lower than that of uncalibrated *macro* case nevertheless consistent with previous estimates [e.g., *Ireson et al.*, 2009]. Figure 4c clearly shows the dominance of S_0 in the BC model as all the relatively low RMSE bars in Figure 4a are associated with S_0 calibration (see red bars in Figure 4c). In addition, calibrated S_0 values for all cases show a consistent constraint around 0.50. Finally, Figure 4d indicates the lack of influence for f_m parameter on model performance.

Figure 5 compares $\Delta\theta_{default}$, $\Delta\theta_{macro}$ and $\Delta\theta$ from the $macro_{opt}$ configuration ($\Delta\theta_{opt}$) with observed soil moisture variability ($\Delta\theta_{obs}$). As mentioned earlier, $\Delta\theta_{default}$ and $\Delta\theta_{macro}$ show considerable discrepancies with $\Delta\theta_{obs}$ while the *macro* configuration exhibits relatively better performance (Figure 3). Figure 5 illustrates that the overall agreement between observed and simulated $\Delta\theta$ improves substantially in case of $macro_{opt}$ compared to *default* and *macro*, which is pronounced especially in the deeper chalk layers. Therefore, this figure indicates that the performance of the BC model in simulating $\Delta\theta$ is further improved by optimizing the K_s and S_0 parameters simultaneously at the Warren Farm site.

As mentioned earlier, efficiently reproducing soil moisture variability over the profile is important due to the fact that $\Delta\theta$ significantly affects water flux and recharge through chalk unsaturated zone. The drainage flux through the bottom of soil column (d_b) of a land surface model can be considered as the potential recharge flux to groundwater [e.g., *Sorensen et al.*, 2014]. Figure 6 compares the daily sum of d_b from the *default* and $macro_{opt}$ configurations at the Warren Farm site. Daily rainfall at this site over the simulation period is shown in Figure 6a. In Figure 6b, the $macro_{opt}$ configuration shows considerable d_b during the colder months, while relatively slow drainage is observed in summer. In contrast, the *default* configuration shows relatively high d_b in summer compared to the colder months. In general, the recharge rate through chalk unsaturated zone during the warmer periods of the year is lower than that in the winter months [*Wellings and Bell*, 1980; *Ireson et al.*, 2009]. Therefore, the $macro_{opt}$ configuration appears to be more consistent with the recharge mechanism in chalk compared to *default*.

In this section, the BC model was evaluated at the point scale. The results showed that in general, the *macro* configuration outperforms the *default* case in simulating $\Delta\theta$. In order to improve the model performance even further, model parameter calibration was performed to

minimize the differences between observed and simulated $\Delta\theta$ at the point scale. In the next sections, the optimized model ($macro_{opt}$) is evaluated at the catchment scale.

4.2. Catchment scale simulations

At the catchment scale, simulation results from the *default* and $macro_{opt}$ configurations are compared with the observations over the Kennet catchment. In order to assess the differences between LE from the *default* and $macro_{opt}$ configurations at the catchment scale, Figure 7 plots spatially averaged 8-day composites of LE from MODIS (LE_{MOD}) against the LE from these configurations ($LE_{default}$ and LE_{opt}, respectively) over Kennet. The agreement between simulated LE and LE_{MOD} is evaluated using the coefficient of determination (R^2, see Appendix) and mean bias. Comparison between $LE_{default}$ and LE_{MOD} shows a coefficient of determination of $R^2_{default} = 0.78$ and a mean bias of $bias_{default} = 10.5$ Wm^{-2}. The agreement between simulated LE and LE_{MOD} improves in case of the $macro_{opt}$ configuration, which is reflected by an increased coefficient of determination of $R^2_{opt} = 0.80$ and a reduced mean bias of $bias_{opt} = 7.1$ Wm^{-2}.

Figure 7 shows considerable differences between $LE_{default}$ and LE_{opt} for relatively high LE, indicating discrepancies especially during the warmer months of the year. Spatially averaged time series of monthly LE_{MOD}, $LE_{default}$ and LE_{opt} is presented in Figure 8a. This figure shows that the differences between $LE_{default}$ and LE_{opt} increases in summer compared to the colder months of the year, which is consistent with Figure 7. Consequently, the *default* configuration underestimates LE in summer compared to LE_{MOD}, which is improved in case of the $macro_{opt}$ configuration. In contrast, the differences between $LE_{default}$ and LE_{opt} are negligible during the colder months of the year.

In addition, Figure 8b compares the observed and simulated monthly average discharge from the two model configurations at the "Kennet at Theale" gauging station (Figure 1a). This

figure depicts that the *default* configuration generally overestimates discharge at this gauging station, which is improved considerably in the case of $macro_{opt}$. We use the Kling-Gupta Efficiency criterion (KGE [*Gupta et al.*, 2009]) to compare the performance of the two model configurations in reproducing observed discharge variability. As mentioned above, the *default* configuration overestimates discharge with $KGE_{default} = -0.17$. On the other hand, the $macro_{opt}$ configuration improves the agreement between observed and simulated discharge, which is reflected by $KGE_{opt} = 0.51$.

In order to summarize the results at catchment scale, Table 4 compares observed and simulated runoff from the two model configurations over the Kennet catchment from 2006-2011. The runoff ratio (*RR*, see Appendix), which is equal to the mean volume of flow divided by the volume of precipitation [e.g., *Kelleher et al.*, 2015], assesses the partitioning of precipitation into runoff over the catchment. The *default* configuration (*RR* = 0.82) shows considerably higher *RR* compared to observation (*RR* = 0.40), indicating overestimation of runoff by the model that is consistent with Figure 8b. Including chalk hydrology in the model remarkably improves the agreement between observed and simulated mean runoff over the Kennet catchment, which is assessed from a runoff ratio of *RR* = 0.46 for the $macro_{opt}$ configuration which is much closer to the observed RR value than *default*.

In Table 4, the relative bias ($\Delta\mu$) of 1.04 between observed and simulated runoff from the *default* configuration again indicates the overestimation by the model. In comparison, $macro_{opt}$ shows a smaller relative bias of $\Delta\mu = 0.12$, indicating improved agreement between observed and simulated mean runoff volume compared to *default*. The relative difference in standard deviation ($\Delta\sigma$, see Appendix) compares the variability of observed and simulated flow in Table 4 relating directly to the seasonal change in runoff. This comparison shows that the *default* configuration overestimates the variability of runoff over the Kennet catchment

386 ($\Delta\sigma$ = 2.04), which is improved in case of *macro* ($\Delta\sigma$ = 0.65). This improvement in
387 reproducing flow variability is also clearly observed in Figure 8b.

388 In this section, the BC model is evaluated using observed mass and energy fluxes over the
389 Kennet catchment. The *default* configuration suggested relatively low summertime LE over
390 the catchment. The agreement between observed and simulated LE was improved in case of
391 the $macro_{opt}$ configuration compared to *default*. It was also observed that the overall runoff
392 prediction was considerably improved by $macro_{opt}$ compared to *default*. Given its simplicity,
393 our results indicate that the proposed parameterization is suitable for use in land surface
394 modelling applications.

395 ## 5. Summary and Conclusions

396 In this study, we proposed a simple parameterization, namely the *Bulk Conductivity* (BC)
397 model to simulate water flow through the matrix-fracture system of chalk in large scale land
398 surface modelling applications. This parameterization was implemented in the Joint UK Land
399 Environment Simulator (JULES) and applied to the Kennet catchment located in the southern
400 UK to simulate the mass and energy fluxes of the hydrological cycle for multiple years. Two
401 model configurations, namely *default* and *macro* were considered with the latter using the BC
402 model to simulate chalk hydrology.

403 The proposed BC model is a single continuum approach of modelling preferential flow [e.g.,
404 *Beven and Germann*, 2013] that involves only 3 parameters, namely the saturated hydraulic
405 conductivity of chalk matrix (K_s), macroporosity factor (f_m) and relative saturation threshold
406 (S_0). Initially, these parameters were estimated from existing literature to assess the
407 performance of the uncalibrated BC model. Finally, the BC model parameters were optimized
408 to minimize the differences between observed and simulated soil moisture variability. Our
409 results indicated that S_0 is by far the most influential parameter in the model when

representing water movement through a soil-chalk column. This highlights the simplicity of the proposed BC model for large-scale studies and potential ease in transferability. In comparison, K_s and f_m showed secondary (low) sensitivity on the model performance. Since this study introduces the BC model, we decided however to take a conservative approach. We optimized K_s and S_0 simultaneously for our catchment scale simulations since this combination resulted in the best overall model performance.

At the catchment scale, the proposed BC parameterization improved simulated latent heat flux (especially in summer) and the overall runoff compared to *default*. Note that the complexity (i.e., number of parameters) of the BC model for simulating water flow through chalk unsaturated zone is substantially lower compared to more commonly used models for this purpose (e.g., dual-porosity models). Despite its simplicity, the proposed parameterization considerably improves the key hydrological fluxes simulated by JULES at the catchment-scale. Therefore, the BC model can potentially be useful for land surface modelling applications over large-scale chalk-dominated areas.

Acknowledgements

We gratefully acknowledge the support by the "A MUlti-scale Soil moisture Evapotranspiration Dynamics study – AMUSED" project funded by Natural Environment Research Council (NERC) grant number NE/M003086/1. The authors would also like to thank Ned Hewitt and Jonathan Evans from the Centre for Ecology and Hydrology (CEH) for providing the data for the point-scale analyses at the Warren Farm. We would also like to thank Miguel Rico-Ramirez (University of Bristol) for helping preparing the precipitation data from the rain gauge network used for the point-scale simulations, Thorsten Wagener (University of Bristol) for his valuable suggestions on model diagnostics, and Joost Iwema (University of Bristol) for helping with the soil samples collected during the 2015 field work

434 campaign. Finally, we would like to thank the reviewers for their comments and suggestions
435 that added to the quality of this manuscript.

436 Appendix

437 Definition of Statistical Metrics

438 Coefficient of determination (R^2) for observation y = y1, …, yn and prediction f = f1, …, fn
439 is defined as

440 $$R^2 = 1 - \frac{SS_{res}}{SS_{tot}}$$

441 where SS_{res} is the residual sum of square and SS_{tot} is the total sum of square. SS_{res} and SS_{tot}
442 are defined as

443 $SS_{res} = \sum_{i=1}^{n}(y_i - f_i)^2$ and

444 $SS_{tot} = \sum_{i=1}^{n}(y_i - \bar{y})^2$ with $\bar{y}$ being the mean of y.

445 Runoff ratio (RR) assesses the portion of precipitation that generates runoff over the
446 catchment. RR is defined as

447 $$RR = \frac{\mu_{runoff}}{\mu_{rain}}$$

448 where μ_{runoff} is mean runoff and μ_{rain} is mean precipitation [e.g., *Kelleher et al.,* 2015].

449 Relative bias ($\Delta\mu$) between observed and simulated time series can be defined as

450 $$\Delta\mu = \frac{\mu_{mod} - \mu_{obs}}{\mu_{obs}}$$

451 where μ_{obs} and μ_{mod} are the mean of observed and simulated time series, respectively. While
452 the optimal value of $\Delta\mu$ is zero, negative (positive) values indicate an underestimation
453 (overestimation) by the model [e.g., *Gudmundsson et al.,* 2012].

Relative difference in standard deviation ($\Delta\sigma$) between observed and simulated time series can be defined as

$$\Delta\sigma = \frac{\sigma_{mod} - \sigma_{obs}}{\sigma_{obs}}$$

where σ_{obs} and σ_{mod} are the standard deviation of observed and simulated time series, respectively [e.g., *Gudmundsson et al.*, 2012].

References

Bakopoulou, C. (2015), Critical assessment of structure and parameterization of JULES land surface model at different spatial scales in a UK Chalk catchment, PhD thesis, Imperial College London, UK, available at: https://spiral.imperial.ac.uk:8443/handle/10044/1/28955.

Bell, V. A. and R. J. Moore (1998), A grid-based flood forecasting model for use with weather radar data: Part 1. Formulation, Hydrol. Earth Syst. Sc., 2, 265-281.

Bell, V. A., A. L. Key, R. G. Jones, and R. J. Moore (2007), Development of a high resolution grid-based river flow model for use with regional climate model output, Hydrol. Earth Syst. Sc., 11, 532-549.

Best, M. J., M. Pryor, D. B. Clark, G. G. Rooney, R. l. H. Essery, C. B. Ménard, J. M. Edwards, M. A. Hendry, A. Porson, N. Gedney, L. M. Mercado, S. Sitch, E. Blyth, O. Boucher, P. M. Cox, C. S. B. Grimmond, and R. J. Harding (2011), The Joint UK Land Environment Simulator (JULES), Model Description – Part 1: Energy and Water Fluxes, Geosci. Model Dev., 4, 677-699.

Beven, K., and P. Germann (2013), Macropores and water flow in soils revisited, Water Resour. Res., 49, 3071–3092.

476 Bloomfield, J. (1997), The role of diagenesis in the hydrogeological stratification of
477 carbonated aquifers: An example from the chalk at Fair Cross, Berkshire, UK, Hydrol. Earth
478 Syst. Sc., 1, 19-33.

479 Blume, T. (2008), Hydrological processes in volcanic ash soils: measuring, modelling and
480 understanding runoff generation in an undisturbed catchment, PhD thesis, Institut für
481 Geoökologie, Universität Potsdam, Potsdam, Germany, available at: https://publishup.uni-
482 potsdam.de/opus4-ubp/files/1524/blume_diss.pdf

483 Brouyère, S. (2006), Modelling the migration of contaminants through variably saturated
484 dual-porosity, dual-permeability chalk, J. Contam, Hydrol., 82, 195-219.

485 Clark, D. B., L. M. Mercado, S. Sitch, C. D. Jones, N. Gedney, M. J. Best, M. Pryor, G. G.
486 Rooney, R. L. H. Essery, E. Blyth, O. Boucher, R. J. Harding, C. Huntingford, and P. M. Cox
487 (2011), The Joint UK Land Environment Simulator (JULES), Model Description – Part 2:
488 Carbon Fluxes and Vegetation Dynamics, Geosci. Model Dev. 4, 701-722.

489 Cox, P. M., R. A. Betts, C. B. Bunton, R. L. H. Essery, P. R. Rowntree and J. Smith (1999),
490 The impact of new land surface physics on the GCM simulation of climate and climate
491 sensitivity, Clim. Dynam., 15, 183-203.

492 Dadson, S. J., I. Ashpole, P. Harris, H. N. Davies, D. B. Clark, E. Blyth, and C. M. Taylor
493 (2010), Wetland inundation dynamics in a model of land surface climate: Evaluation in the
494 Niger inland delta region, J. Geophys. Res., 115.

495 Dadson, S. J., V. A. Bell, and R. G. Jones (2011), Evaluation of a grid based river flow model
496 configured for use in a regional climate model, J. Hydrol., 411, 238-250.

497 Dettinger, M. D., and H. F. Diaz (2000), Global characteristics of streamflow seasonality and
498 variability, J. Hydrometeorol., 1, 289-310.

499 Essery, R., M. Best, and P. Cox (2001), MOSES 2.2 technical documentation (Hadley Centre
500 technical note 30), Hadley Centre, Met Office, UK.

501 Garcia, M., C. D. Peters-Lidard, and D. C. Goodrich (2008), Spatial interpolation of
502 precipitation in a dense gauge network for monsoon storm events in the southwestern United
503 States, Water Resour. Res., 44.

504 Gascoin, S., A. Duchare, P. Ribstein, M. Carli, and F. Habtes (2000), Adaptation of a
505 catchment-based land surface model to the hydrological setting of the Somme River basin
506 (France), J. Hydrol., 368, 105-116.

507 Gudmundsson, L., T. Wagener, L. M. Tallaksen, and K. Engeland (2012), Evaluation of nine
508 large-scale hydrological models with respect to the seasonal runoff climatology in Europe,
509 Water Resour. Res., 48.

510 Gupta, H. V., H. Kling, K. K. Yilmaz, and G. F. Martinez (2009), Decomposition of the mean
511 squared error and NSE performance criteria: implications for improving hydrological
512 modelling, J. Hydrol., 377, 80-91.

513 Haria, A. H., M. G. Hodnett, and A. C. Johnson (2003), Mechanisms of groundwater
514 recharge and pesticide penetration to chalk aquifer in southern England, J. Hydrol., 275, 122-
515 137.

516 Hartmann, A., N. Goldscheider, T. Wagener, J. Lange, and M. Weiler (2014), Karst water
517 resources in a changing world: Review of hydrological modeling approaches, Rev. Geophys.,
518 52, 218–242, doi:10.1002/2013RG000443.

519 Hewitt, N., M. Robinson, and D. McNeil (2010), Pang and Lambourn hydrometric review
520 2009, Wallingford, NERC/Centre for Ecology and Hydrology, (CEH project number:
521 C04076).

522 Ireson, A. M., S. A. Mathias, H. S. Wheater, A. P. Butler and J. Finch (2009), A model for
523 flow in the chalk unsaturated zone incorporating progressive weathering, J. Hydrol., 365,
524 244-260.

525 Ireson, A. M. and A. P. Butler (2011), Controls on preferential recharge to chalk aquifers, J.
526 Hydrol., 398, 109-123.

527 Ireson, A. M. and A. P. Butler (2013), A critical assessment of simple recharge models:
528 application to the UK chalk, Hydrol. Earth Syst. Sc., 17, 2083-2096.

529 Ireson, A. M., H. S. Wheater, A. P. Butler, S. A. Mathias, J. Finch, and J. D. Cooper (2006),
530 Hydrological processes in the chalk unsaturated zone – insight from an intensive field
531 monitoring program, J. Hydrol., 330, 29-43.

532 Ireson, A. M., S. A. Mathias, H. S. Wheater, A. P. Butler, and J. Finch (2009), A model for
533 flow in the chalk unsaturated zone incorporating progressive weathering, J. Hydrol., 365,
534 244-260.

535 Jackson, C. and Spink, A. (2004) User's Manual for the Groundwater Flow Model
536 ZOOMQ3D, IR/04/140, British Geological Survey, Nottingham, UK.

537 Kelleher, C., T. Wagener, and B. McGlynn (2015), Model-based analysis of the influence of
538 catchment properties on hydrologic partitioning across five mountain headwater
539 subcatchments, Water Resour. Res., 51, 4109-4136.

Kling, H., M. Fuchs, and M. Paulin (2012), Runoff conditions in the upper Danube basin under an ensemble of climate change scenarios. Journal of Hydrology, Volumes 424-425, 6 March 2012, 264-277.

Lehner, B., K. Verdin, and A. Jarvis (2008), New global hydrography derives from spaceborne elevation data, EOS, Transactions, AGU, 89(10), 93-94.

Le Vine, N., A. Butler, N. McIntyre, and C. Jackson (2016), Diagnosing hydrological limitations of a land surface model: application of JULES to a deep-groundwater chalk basin, Hydrol. Earth Syst. Sc., 20, 143-159.

Lee, L. J. E., D. S. L. Lawrence, and M. Price (2006), Analysis of water-level response to rainfall and implications for recharge pathways in the chalk aquifer, SE England, J. Hydrol., 330, 604-620.

Ly, S., C. Charles, and A. Degré (2013), Different methods for spatial interpolation of rainfall data for operational hydrology and hydrological modeling at watershed scale. A review, Biotechnol. Agron. Soc. Environ. 17, 392-406.

Mathias, S. A., A. P. Butler, B. M. Jackson, and H. S. Wheater (2006), Transient simulations of flow and transport in the chalk unsaturated zone, J. Hydrol., 330, 10-28.

Met Office (2006), UK hourly rainfall data, Part of the Met Office Integrated Data Archive System (MIDAS), NCAS British Atmospheric Data Centre, 21 March 2016, http://catalogue.ceda.ac.uk/uuid/bbd6916225e7475514e17fdbf11141c1.

Morton, D., C. Rowland, C. wood, L. Meek, C. Marston, G. Smith, R. Wadsworth, and I. C. Simpson (2011), Final report for LCM2007 – the new UK Land Cover Map (CS technical report no 11/07), Centre for Ecology and Hydrology, UK.

562 Mu, Q., F. A. Heinsch, M. Zhao, and S. W. Running (2007), Development of a global
563 evapotranspiration algorithm based on MODIS and global meteorology data, Remote Sens.
564 Environ., 111, 519-536.

565 Price, A., R. A. Downing, and W.M. Edmunds (1993), The chalk as an aquifer. In: Downing,
566 R. A., M. Price, and G. P. Jones *The hydrogeology of the chalk of north-west Europe*. Oxford:
567 Claredon Press. 35-58.

568 Price, M., R. G. Low, and C. McCann (2000), Mechanisms of water storage and flow in the
569 unsaturated zone of chalk aquifer, J. Hydrol., 54-71.

570 Rawls, W. J., D. L. Brankensiek, and K. E. Saxton (1982), Estimation of soil water
571 properties, Trans. ASAE, 25(5), 1316–1320.

572 Robinson, E. L., E. Blyth, D. B. Clark, J. Finch, and A. C. Rudd (2015), Climate hydrology
573 and ecology research support system potential evapotranspiration dataset for Great Britain
574 (1961- 2012) [CHESS-PE], NERC-Environmental Information Data Centre.

575 Schär C., D. Lüthi, U. Beyerle, and E. Heise (1999), A soil precipitation feedback: A process
576 study with a regional climate model, J. Clim., 12, 722–741.

577 Schaap, M. G., and F. J. Leij (1998), Database-related accuracy and uncertainty of
578 pedotransfer functions, Soil Sci., 163(10), 765–779.

579 Sorensen, J. P. R., J. W. Finch, A. M. Ireson, and C. R. Jackson (2014), Comparison of varied
580 complexity models simulating recharge at the field scale, Hydrol. Process., 28, 2091-2102.

581 Van den Daele, G. F. A., J. A. Barker, L. D. Connell, T. C. Atkinson, W. G. Darling, and J.
582 D. Cooper (2007), J. Hydrol., 342, 157-172.

583 Van Genuchten, M. Th. (1980), A closed-form equation for predicting the hydraulic
584 conductivity of unsaturated soils, Soil Sci. Soc. Am. J., 44, 892–898.

585 Walters, D. N., K. D. Williams, I. A. Boutle, A. C. Bushell, J. M. Edwards, P. R. Field, A. P.
586 Lock, C. J. Morcrette, R. A. Stratton, J. M. Wilkinson, M. R. Willett, N. Bellouin, A. Bodas-
587 Salcedo, M. E. Brooks, D. Copsey, P. D. Earnshaw, S. C. Hardiman, C. M. Harris, R. C.
588 Levine, C. MacLachlan, J. C. Manners, G. M. Martin, S. F. Milton, M. D. Palmer, M. J.
589 Roberts, J. M. Rodríguez, W. J. Tennant, and P. L. Vidale (2014), The Met Office unified
590 model global atmosphere 4.0 and JULES global land 4.0 configurations, Geosci. Model Dev.,
591 7, 361-386.

592 Welliings, S. R., and J. P. Bell (1980), Movement of water and nitrate in the unsaturated zone
593 of upper chalk near Winchester, Hants., England, J. Hydrol, 48, 119-136.

594 Williams, K., and D. Clark (2014), Disaggregation of daily data in JULES (Hadley Centre
595 technical note 96), Hadley Centre, Met Office, UK.

596 Zehe, E. and G. Blöschl (2004), Predictability of hydrologic response at the plot and
597 catchment scales: Role of initial conditions, Water Resour. Res, 40.

598 Zehe, E., T. Maurer, J. Ihringer, and E.Plate (2001), Modeling water flow and mass transport
599 in a loess catchment, Phys. Chem. Earth (B), 26, 487-507.

600 Zehe, E., U. Ehret, T. Blume, A. Kleidon, U. Scherer, and M. Westhoff (2013), A
601 thermodynamic approach to link self-organization, preferential flow and rainfall-runoff
602 behaviour, Hydrol. Earth Syst. Sc., 17, 4297-4322.

603

604

Tables

Table 1. Field measurements and remote sensing data.

Data	Spatial scale	Temporal extent	Frequency	Source
Soil moisture	Point[a]	2003-2005	15 day	N. Hewitt (CEH)
Latent heat flux	Global	2006-2011	8 day, 1 month	MODIS
Discharge	Point[b]	2006-2011	1 day	NRFA

[a]Measured at Warren Farm.
[b]Locations are shown in Figure 1a.

Table 2. Hydraulic properties for different soil types (refer to Figure 1c). Saturated hydraulic conductivity (K_s) and porosity data are obtained from *Rawls et al.* [1982]. The Van Genuchten parameters are acquired from *Schaap and Leij* [1998].

Texture	K_s (mmd^{-1})	Porosity (-)	α (m^{-1})	n (-)
Loam	320	0.463	3.33	1.56
Silt loam	172	0.50	1.2	1.39
Clay	15	0.475	2.12	1.2

Table 3. Hydraulic properties of chalk

Properties	Uncalibrated		Range for calibration	Calibrated value
	Value	Source		
K_s (mmd^{-1})	1.0	Price et al., 1993	0.2 - 5.0	0.31
S_0 (-)	0.8	Observations	0.0 - 1.0	0.46
f_m (-)	10^5	Price et al., 1993	10^4 - 10^6	10^{5*}
α (m^{-1})	3.0	Le Vine et al., 2016	-	-
n (-)	1.4	Le Vine et al., 2016	-	-

* f_m parameter not calibrated

Table 4. Comparison between observed and simulated daily average runoff from the two configurations over the Kennet catchment. Metrics include the Runoff Ratio (RR), relative bias ($\Delta\mu$), and relative difference in standard deviation ($\Delta\sigma$) (refer to appendix for further information).

Metric	Observed	Simulated (*default*)	Simulated (*macro*)
RR	0.40	0.82	0.46
$\Delta\mu$	-	1.04	0.12
$\Delta\sigma$	-	2.04	0.65

Figures

Figure 1. (a) Location, (b) vegetation cover and (c) soil texture over the study area. The red line in (a) outlines the Kennet catchment boundary, while the river network is shown in blue. The black triangle in (a) shows the location of the discharge gauging station at the catchment outlet and the black square corresponds to Warren Farm location where point-scale simulations are carried out. The black line in (c) encloses the area of the catchment where chalk is present.

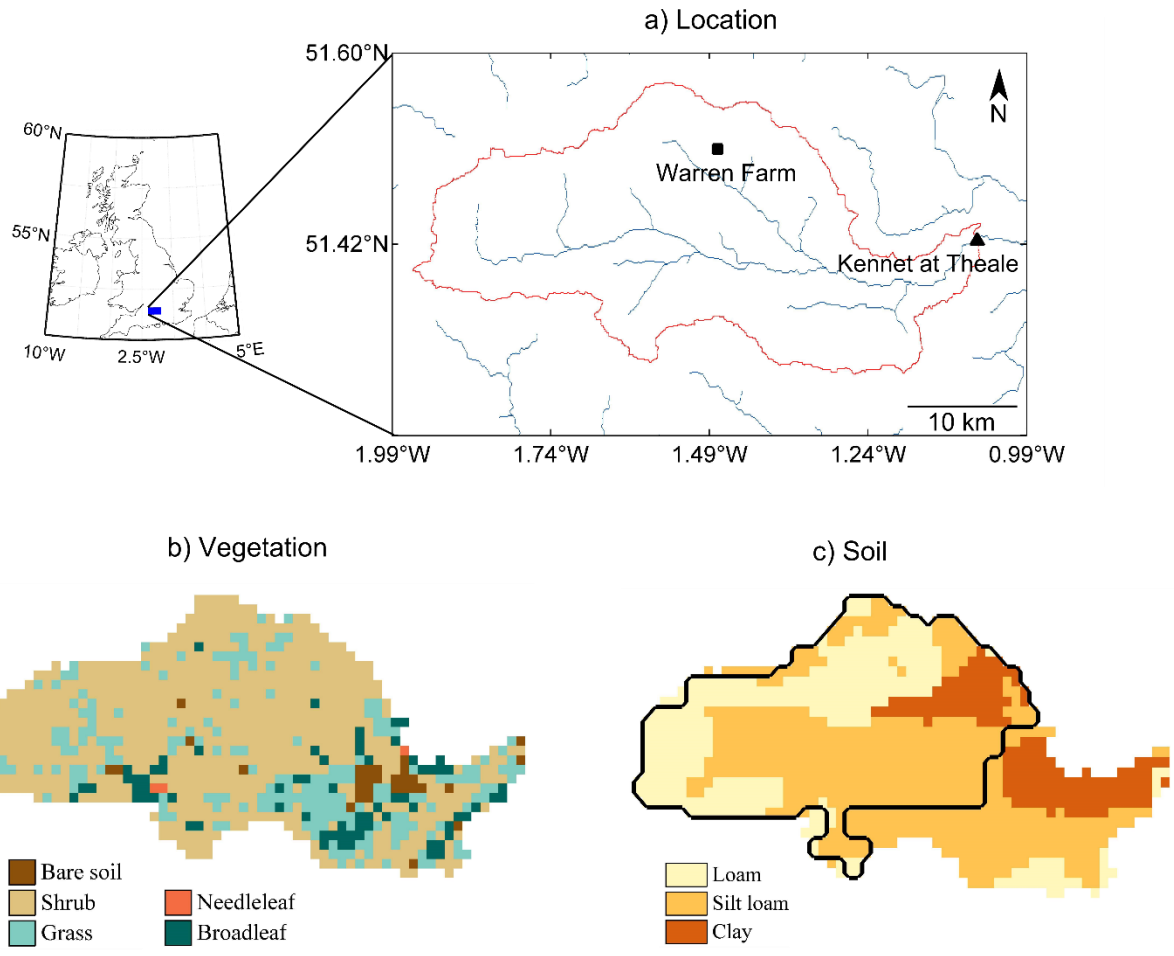

Figure 2. (a) Example of soil profiles collected at Warren Farm during a field campaign in 2015 and (b) the two model configurations.

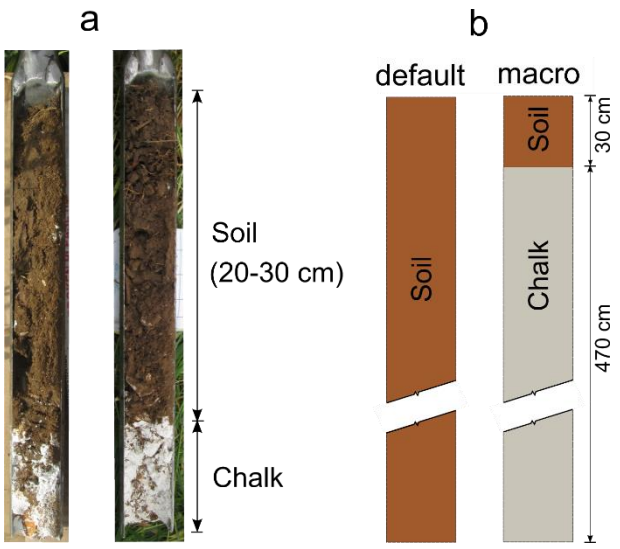

Figure 3. Comparison between observed and simulated (a) soil moisture (θ) and (b) change in soil moisture ($\Delta\theta$) from the *default* and *macro* configurations at a depth of 2 m below land surface at the Warren Farm site. The shaded areas constructed from 2 soil moisture probes at the Warren Farm site denote the range of observed data in these plots.

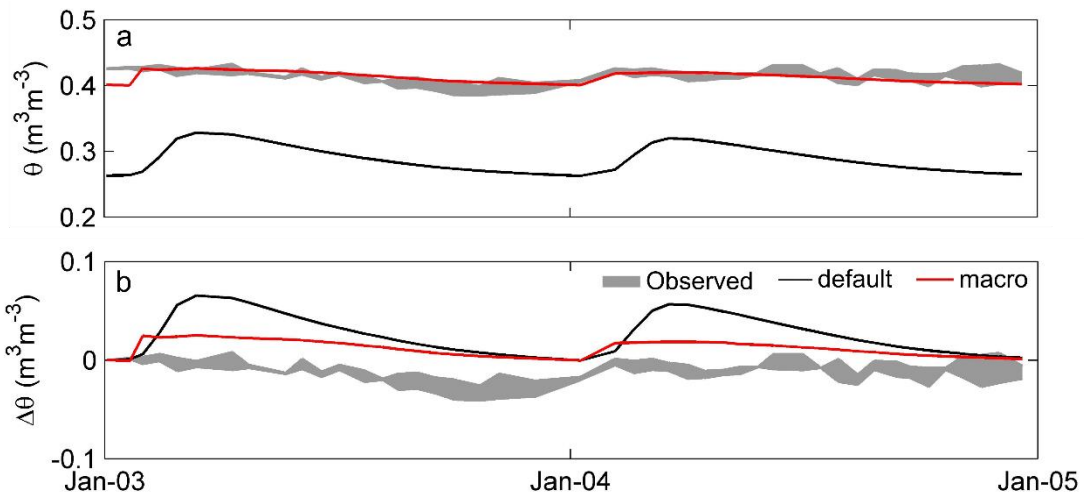

Figure 4. (a) Model performance in reproducing observed and simulated $\Delta\theta$, (b) K_s, (c) S_0 and (d) f_m for different parameter combinations considered in the optimization. For each parameter (i.e., panels b, c, and d), red bars show cases in which the relevant parameter is calibrated (either individually or in combination with others); while the blue bars correspond to cases in which the selected parameter is not calibrated (i.e., fixed value according to literature as in the *macro* case). Note that except for the *default* and *macro*, the simulation yielding the lowest RMSE (out of 2,000 model runs) is presented in this plot.

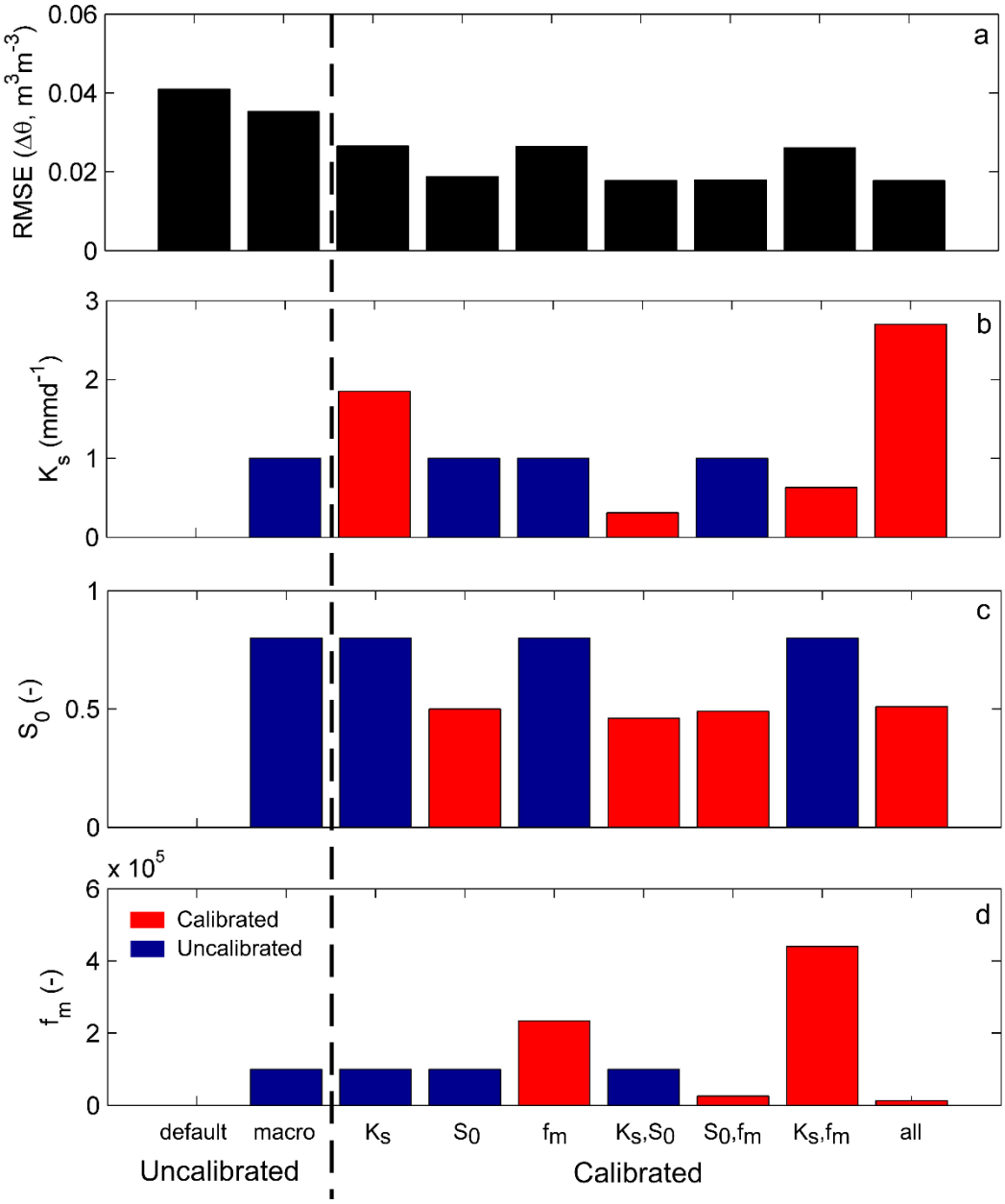

669 Figure 5. Comparison between observed and simulated $\Delta\theta$ from *default*, *macro* and *macro*$_{opt}$

670 configurations at various depths below land surface. The shaded areas, which are constructed

671 from 2 soil moisture probes at the Warren Farm site, denote the range of $\Delta\theta$.

672

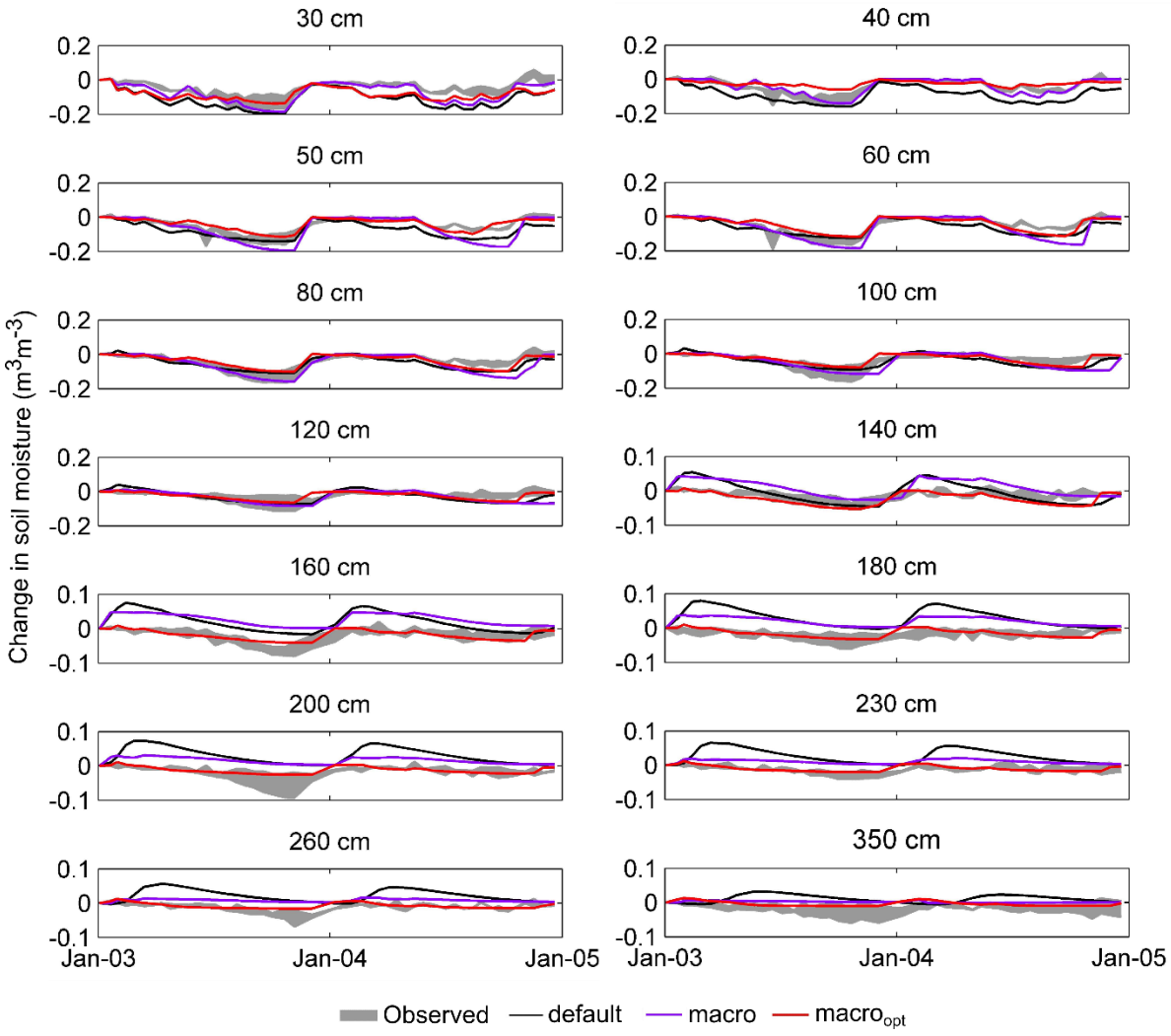

673

674

675

676

677

678

679 Figure 6. (a) Daily precipitation and (b) daily drainage through the bottom of the soil column

680 at Warren Farm over the two simulated years (2003-2005).

681

682

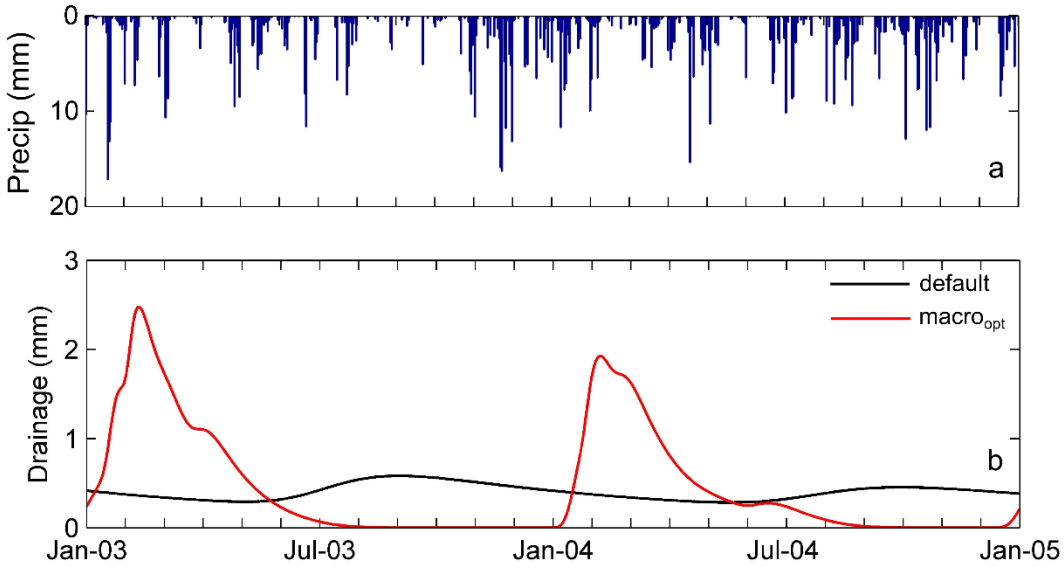

683

684

685

686

687

688

689

690

691

692

Figure 7. Catchment average 8 day composites of MODIS estimated *LE* (LE_{MOD}) against simulated *LE* from *default* and *macro* configurations ($LE_{default}$ and LE_{macro}, respectively) along with the linear models fitted for $LE_{default}$ (black line) and LE_{macro} (red line). The 1:1 line is shown in grey, which represents the perfect fit between LE_{MOD} and simulated *LE*.

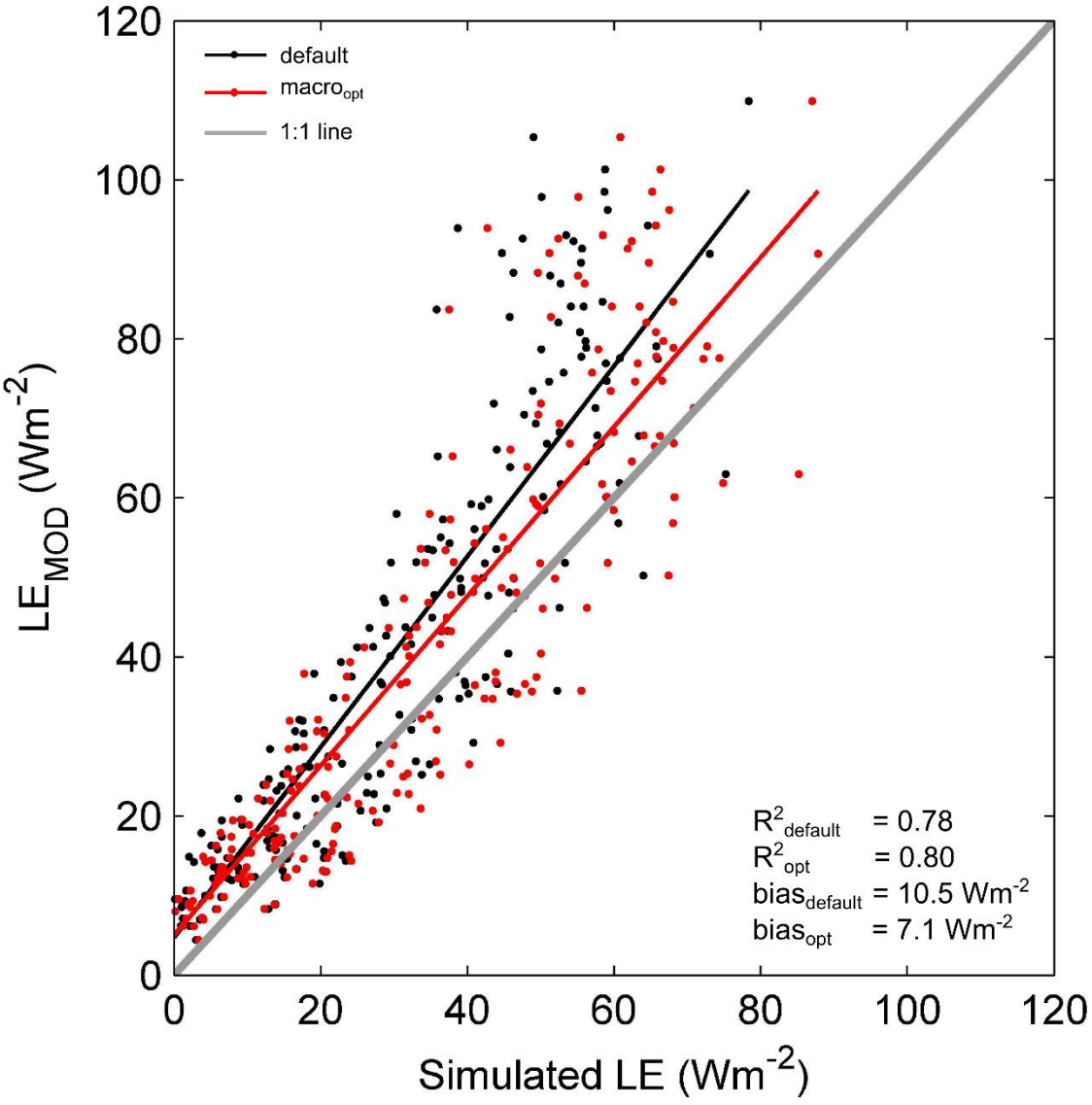

Figure 8. (a) Spatially averaged monthly latent heat flux (*LE*) from MODIS, *default* and *macro*$_{opt}$ configurations over the Kennet catchment and (b) monthly average observed and simulated discharge from the *default* and *macro*$_{opt}$ configurations at the "Kennet at Theale" gauging station.